Chemistry Africa
https://doi.org/10.1007/s42250-024-01112-z

ORIGINAL ARTICLE

Green Clay Materials Applied in Packed Bed Columns for the Hexavalent Chromium Adsorption from Aqueous Solutions

Mabrouk Eloussaief[1] · Nesrine Dammak[1] · Sana Ghrab[1] · Olfa Ouled Ltaief[1] · Wiem Hamza[1] · Stephanie Lambert[2] · Hicham Zaitan[3] · Mourad Benzina[1]

Received: 9 May 2024 / Accepted: 20 October 2024

Abstract
The removal of hazardous metal ions from polluted water is a crucial process aimed at enhancing water quality. In this study, we conducted a dynamic adsorption investigation utilizing natural green clay for the removal of hexavalent chromium from aqueous solutions. The material underwent characterization through various techniques, including fluorescence spectrometry (XRF), X-ray diffraction (XRD), Fourier transform infrared spectroscopy (FTIR) and nitrogen-physisorption (BET). Column tests of green clay material and sand mixtures were performed to evaluate sorption in dynamic systems. Adsorption conditions were examined by varying the initial Cr^{6+} concentration, flow rate and column height. The maximum purification was achieved at a concentration of 50 mg/L, a flow rate of 3mL/min and a bed height of 12 cm.

The mathematical models of Bohart-Adams, Thomas, and Yoon-Nelson were employed to analyze experimental data and predict breakthrough curves in continuous adsorption. Through comparison of R^2 values, it was determined that the Yoon-Nelson and Thomas diffusion models effectively capture and accurately describe the experimental data.

The results obtained indicate a potential expansion of fixed-bed adsorption for the heavy metals treatment in industrial-scale wastewater. Additionally, the natural green clay material exhibited remarkable reusability and showed promising characteristics for various environmental and industrial applications.

Keywords Green clay · Characterization · Hexavalent chromium · Adsorption · Fixed bed column · Modeling

1 Introduction

Among all pollutants, heavy metals are of paramount concern due to their toxic nature and the potential risk of accumulation in living organisms through food chains [1–3]. For instance, hexavalent chromium Cr(VI) is a highly toxic heavy metal, with a maximum permissible quantity of 0.05 mg/L in potable water, as per the Environmental Protection Agency (EPA) guidelines [4–7]. It primarily emanates from industrial processes such as metal processing, metal mining and smelting, electroplating, leather and dyeing, among others [8, 9]. Adverse health effects associated

✉ Mabrouk Eloussaief
eloussaiefmabrouk@yahoo.fr

Nesrine Dammak
dammak.nes@gmail.com

Sana Ghrab
ghrab.sana@yahoo.fr

Olfa Ouled Ltaief
olfa.ol@live.fr

Wiem Hamza
hamzawiem@gmail.com

Stephanie Lambert
stephanie.lambert@ulg.ac.be

Hicham Zaitan
hicham.zaitan@usmba.ac.ma

Mourad Benzina
mourad.benzina@enis.rnu.tn

[1] Laboratoire de Recherche Eau, Energie et Environnement (LR3E), Code: LR99ES35, Ecole Nationale d'Ingénieurs de Sfax, Université de Sfax, B.P1173.W.3038, Sfax, Tunisie

[2] Laboratory of Chemical Engineering - Catalytic Engineering Institute of Chemistry, University of Liege, Liege, Belgium

[3] Processes, Materials and Environment Laboratory (LPME), Department of Chemistry, Faculty of Sciences and Technology of Fez, Sidi Mohamed Ben Abdellah University, Fez, Morocco

Published online: 05 November 2024

with Cr(VI) exposure include nasal and skin irritation, eardrum perforation, and lung carcinogenesis [10–12].

Currently, various water treatment methods, including ion exchange, reverse osmosis, membrane separation, coagulation and flocculation, chemical sedimentation, and adsorption, have been employed for the removal of heavy metals [13–17]. Therefore, there is a need for exploring new alternatives and advancements in heavy metal treatment [18–21]. While most studies on heavy metal sorption by clay materials have been conducted in batch setups, fewer studies address adsorption in dynamic systems.

Continuous adsorption using different materials is an emerging alternative method due to its cost-effectiveness, simplicity in design and operation, capability for removal at low concentrations, low sludge production, and environmental friendliness [22–25].

Despite its higher adsorption capacity, activated carbon is considered a very expensive material, both in terms of preparation and purchase. Therefore, there is an attempt to identify low-cost materials that can be used as adsorbents, sourced from green materials without chemical treatments [26–28]. The term "green adsorbent" refers to materials derived from agricultural waste, natural sources, etc., that are low-cost, abundant, and environmentally benign, suitable for adsorption [29]. Studies have reported the use of clay minerals [30, 31] biomass waste [32, 33], activated carbon [34–36] for the removal of contaminants from water. Clay materials are considered highly promising and cost-effective adsorbents [37, 38]. They have been extensively studied for their effectiveness in adsorption processes and have found applications in various industries in their natural state [39]. Some papers have demonstrated the practical application of natural clay material as a conventional and low-cost adsorbent [40–42]. The objective of this study is to valorize a significant deposit of green clay material located in the southern part of Tunisia and investigate its adsorption capacity for hexavalent chromium in a fixed bed from an aqueous solution. This clay material, primarily composed of illite, is being utilized for the first time in a fixed bed column as a clean technology for the polluted water treatment.

2 Geological Setting

The Gabes governorate holds significant potential in terms of natural resources and geological features, playing a crucial role in the country's economic cycle [43–45]. This study places a specific focus on the clay quarries within Bouhedma formation, particularly those located at Jbel Zemlet El Beida in the El Hamma region (Fig. 1). The Barremian series displays alternating layers of red and green clays, ranging in thickness from metric to decametric scales (Fig. 1). The clay fraction primarily consists of 60 to 80% illite, kaolinite, and occasionally chlorite [46, 47]. While red clay materials are widely utilized in brick manufacturing, the economic importance of green clays from the same site has been largely overlooked. This research seeks to bring attention to the potential of these green clays and to explore their effectiveness in treating polluted water.

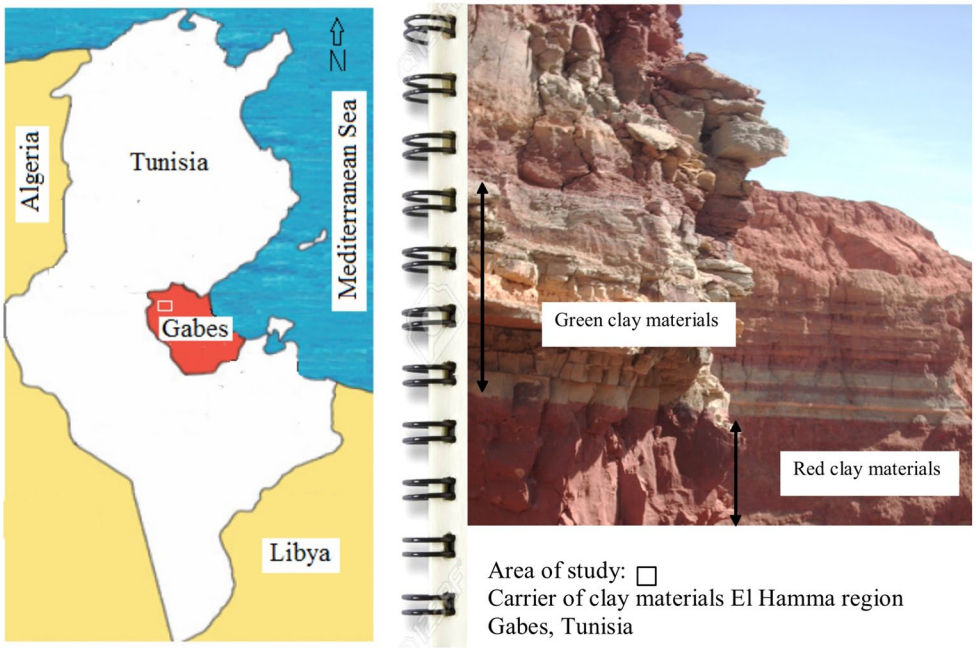

Fig. 1 Geological setting of collected sample

3 Materials and Methods

3.1 Material

The green clay material (GCM) collected from the El Hamma region (Gabes, Tunisia) was used in its natural form without any chemical treatment and was sieved through a metallic sieve between mesh sizes of 200 and 500 µm. The second material used in this study was sand, also collected from southern Tunisia, specifically from the Wetherf region. The purpose of using sand is to prevent clogging of the column. The final material used is wool, which serves as a support for the packed column.

3.2 Methods

The characterization of the collected sample involved the utilization of various experimental methods. The chemical analysis was determined by fluorescence spectrometry using a Thermo Scientific device Niton FXL FM-XRF analyzer at mineralogical laboratory of our department, (Faculty of Sciences, Sfax, Tunisia). The identification of functional groups within the green clay material was accomplished through the utilization of an FTIR analyzer (Shimadzu IRAffinity-1 S, Tokyo, Japan). To analyze the mineralogical composition of the green clay material, XRD analysis was employed. A Philips PW 1710 X-ray diffractometer (Japan) utilizing CuKα (λ = 1.54056 Å) radiation was employed over a range of 2θ angles from 10 to 60, with a scan rate of 1°/min at room temperature. The BET surface area of the sample was determined by employing a nitrogen adsorption-desorption analyzer, specifically the ASAP 2020 V3.04 H instrument from Micromeritics, France. The loss on ignition (L.O.I.) of the sample was determined through calcination at 1000 °C, following the procedure outlined by Eloussaief et al. (2009) [48]. Pore volume and porosity measurements were conducted using pycnometry in the laboratory.

4 Experimental Procedure

A fixed-bed column was specifically designed for conducting continuous adsorption experiments in the laboratory. The experimental setup and a simplified schematic utilized in this study are illustrated in Fig. 2.

The column adsorption tests were carried out utilizing a glass column with dimensions of 19 cm in height and 2.6 cm in diameter. The column was packed with a mixture of green clay material and sand, maintaining a ratio of 2. A synthetic wastewater containing hexavalent chromium was introduced into the column through a peristaltic pump, ensuring a controlled flow rate. Hexavalent chromium solutions were prepared using a laboratory stock of K_2CrO_4 (Sigma Aldrich, St. Louis, MO, USA, purity ≥ 99%). The solution was prepared by dissolving 0.2 g of dried potassium chromate in distilled water.

The purification percentage of chromium ions and adsorption capacity, q (mg/g), were calculated using the following equations:

$$\%Purification = \frac{C_0 - C}{C_0} 100 \quad (1)$$

$$q = \frac{(C_0 - C)}{M} V \quad (2)$$

Where, C_0 and C are the initial and outlet concentration of chromium ions in mg/L, respectively. V is the volume of the solution and M is the mass of the adsorbent (g). A calorimetric UV-visible spectrophotometer (UV-1650PC model, Shimadzu, Japon) was employed to measure the Cr^{6+}concentration in the outlet of each sample at 540 nm [49].

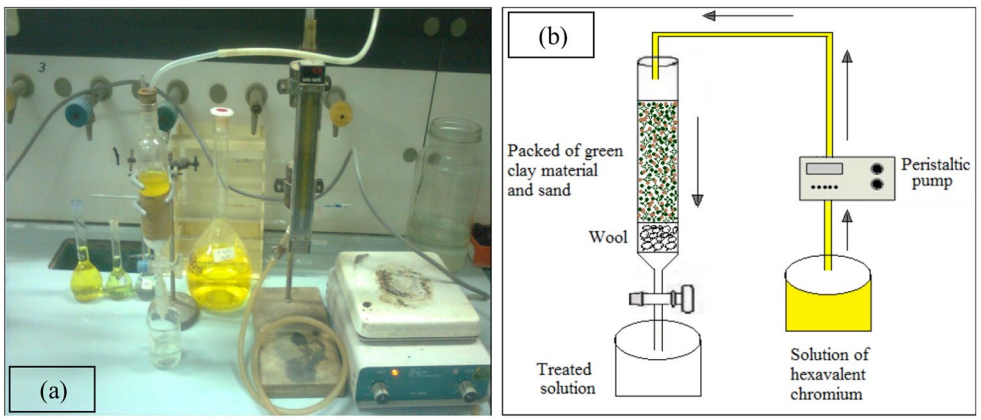

Fig. 2 Exeprimental setup (**a**) and simplified schema of fixed bed adsorption (**b**)

5 Mathematical Models

The breakthrough curves are defined by the shape of the front and the breakthrough time, which marks when the pollutant concentration ceases to be zero at the column's exit. According to [50–53], curve modeling involves predicting breakthrough times, saturation times, and the shape of the front. The physicochemical characteristics of the adsorbent and the fluid to be adsorbed, along with parameters such as initial concentration, bed height, and flow rate, determine the form of the breakthrough curves and the piercing times.

As a general principle, material balance equations typically lack a straightforward analytical solution, necessitating the application of digital resolution methods. The fixed-bed adsorption model presents a certain level of complexity in obtaining an analytical solution. These models play a crucial role in designing and predicting the performance of fixed-bed adsorption processes. Various models exist for breakthrough curves, including classic models and those tailored by researchers for highly specific applications. The performance of the adsorption column was characterized using parameters derived from the Bohart-Adams, Thomas, and Yoon-Nelson models.

5.1 Bohart-Adams

Bohart and Adams pioneered breakthrough curve modeling in 1920 [54]. Their model assumes that the adsorption rate is proportional to both the remaining adsorbent capacity and the concentration of adsorbed species. Fluid-solid interactions are described by the Langmuir equation, and the adsorption rate is constrained by the surface area of the material, i.e., external mass transfer. The reaction equation is expressed as follows [51]:

$$\frac{C}{C_0} = \exp\left(k_{BA}.C_0.t - \frac{k_{BA}.N_0.Z}{u}\right) \tag{3}$$

with,

C: the concentration of the solute ($kg.m^{-3}$);

C_0: the initial solution concentration ($kg.m^{-3}$);

k_{BA}: the adsorbent-adsorbent adsorption kinetic constant ($m^3.kg^{-1}.min^{-1}$);

N_0: maximum volumetric absorption capacity ($kg.m^{-3}$);

u: the migration speed ($m.min^{-1}$);

Z: the height of the absorbent bed (m).

5.2 Thomas

The Thomas model is widely employed for predicting breakthrough curve parameters. It enables the calculation of the adsorbent's adsorption capacity, which is instrumental in effectively designing an adsorption process [51, 53]. This model can be described by the following expression:

$$\frac{C}{C_0} = \frac{1}{1 + \exp\left(\frac{k_{Th}}{Q}\left(q_0 \cdot m - C_0 \cdot Q \,.\, t\right)\right)} \tag{4}$$

where,

k_{Th}: Thomas' constant in ($m^3.kg^{-1}.s^{-1}$);

q_0: maximum adsorption capacity ($kg.kg^{-1}$).

5.3 Yoon-Nelson Model

This model is based on a decrease in the probability of adsorption for adsorbed molecules with the adsorbent congestion. This model does not require details about the type of adsorbent or the characteristics of the adsorbed and the physical properties of the fixed adsorbing bed [51, 53]. For single component adsorption, the Yoon and Nelson model is expressed as follows:

$$\frac{C}{C_0} = \frac{1}{1 + \exp\left(k_{YN}\left(t_{50} - t\right)\right)} \tag{5}$$

with.

k_{YN}: Yoon and Nelson constant (min^{-1});

t50: time at which 50% of the liquid entering the column is at column exit.

The calculation of theoretical breakthrough curves requires the determination of K_{YN} and t50 for the adsorbate to be adsorbed. These values are determined experimentally.

6 Results and Discussions

6.1 Characterization

6.1.1 Physico-Chemical Analysis

Physico-chemical analyses of GCM are presented in Table 1. The sample predominantly comprises silica (46.67%) and alumina (25.7%). Additionally, other significant oxides including CaO, MgO, K_2O, and Na_2O are detected. The presence of the potassium ion, functioning as a load balancer, suggests its possible occurrence in the leaf inter-layer of illite. The material exhibits a loss on ignition of 15.2% and a porosity of 34% (Table 1).

6.1.2 DRX Analysis

The diffractogram presented in Fig. 3 illustrates the mineralogical analysis of GCM sample obtained from the

Table 1 Chemical and physical characteristics of the green clay material (in mass %)

	Chemical composition							Textural properties				
Oxides (%)	SiO_2	Al_2O_3	Fe_2O_3	CaO	MgO	K_2O	Na_2O	LOI	Vp	Ps	χ	S_{BET}
GCM	46.67	25.7	3	2.41	2.16	2.45	1.58	15.2	0.18	8.23	34	67

LOI: Loss On Ignition; Vp: Volume of pore (cm^3/g); Ps: Pore size (nm); χ: Porosity (%); S_{BET}: Specific surface of BET (m^2/g)

Bouhedma formation located in Jebel Aziza, South Tunisia. The mineralogical analysis of the sample reveals distinctive peaks indicative of clay minerals. Illite exhibits a peak at 9.975 Å for d(001) basal spacing, a characteristic feature of Cretaceous-aged Tunisian clay, as previously documented by Sdiri et al. [55] and Ghrab et al. [56]. Additionally, a characteristic peak of kaolinite is observed at 7.160 Å, consistent with prior research [57]. The presence of clays is associated with other minerals, such as Quartz, identified by reflections at 3.341 Å. Furthermore, a minor fraction of dolomite is inferred from the faint peak occurring at 2.282 Å.

6.1.3 FTIR Analysis

The loading spectrum of GCM is illustrated in Fig. 4 and encompasses the following FTIR spectral bands: two stretching bands associated with structural hydroxyl groups (3691 and 3619 cm^{-1}), a band corresponding to Si-O stretching (987 cm^{-1}), deformation bands related to Al-Al-OH vibration (987 cm^{-1}), and deformation bands associated with Al-O-Si in-plane vibration (797 cm^{-1}) [27]. The bands observed at 3619 cm^{-1}, 987 cm^{-1}, and 797 cm^{-1} are attributed to illite, similar results were found in the study reported by Oumar et al. in 2022 [58]. The bands at 1638 and 1634 cm^{-1} in the loading spectra are indicative of carbonates present as impurities in the sample [59]. The presence of carbonates in this sample is minimal; hence, the intensity of the band in the IR spectra is very weak. The FTIR findings are consistent with the results obtained from the DRX analysis.

6.1.4 BET Analysis

The N2 adsorption/desorption isotherm for the adsorbent sample is shown in Fig. 5. The relative pressure (P/P_0) for the studied material (Fig. 5) ranges from 0.35 to 0.98, corresponds to the base of the hysteresis loop, and signifies the start of capillary condensation in the thinnest pores. As the P/P_0 approaches 1, a sharp increase in the sorption curves can be observed, indicating the presence of larger pores in the material. In this work, the relative pressure range too, from 0.35 to 0.98 a rapid absorption takes place, suggesting the presence of empty voids in the crystalline structure of the clay mineral [60]. Additionally, the sorption-desorption hysteresis clearly shows that liquid nitrogen is condensed in the mesopores of GCM. The limited absorption over a range of high P/P_0 and capillary condensation occurring in mesopores are the causes of the observed hysteresis [61, 62]. The IUPAC classification allows the hysteresis to be categorized as type H2 [63]. Table 1 shows the properties of

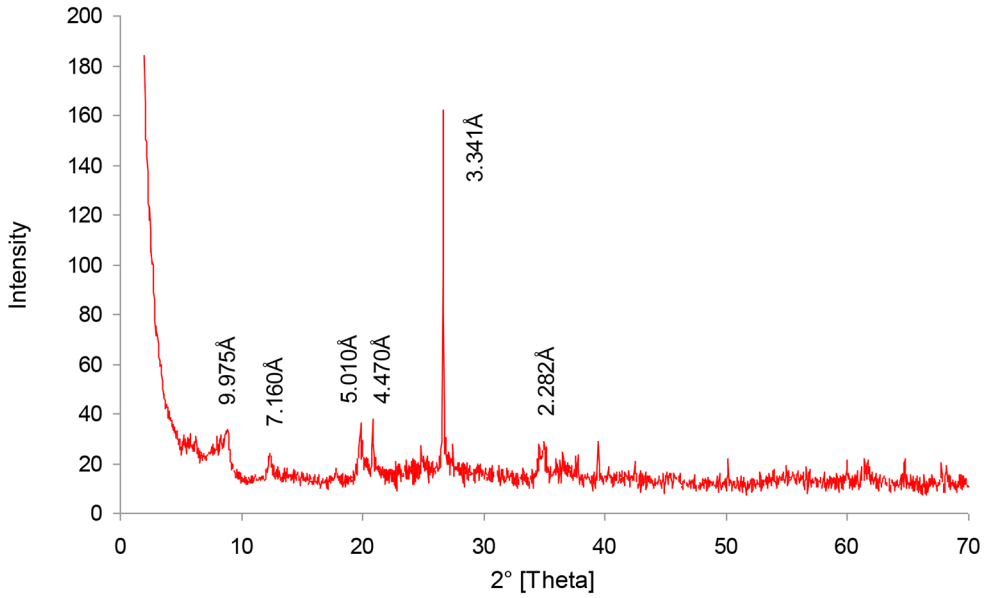

Fig. 3 XRD diffractogram of green clay material

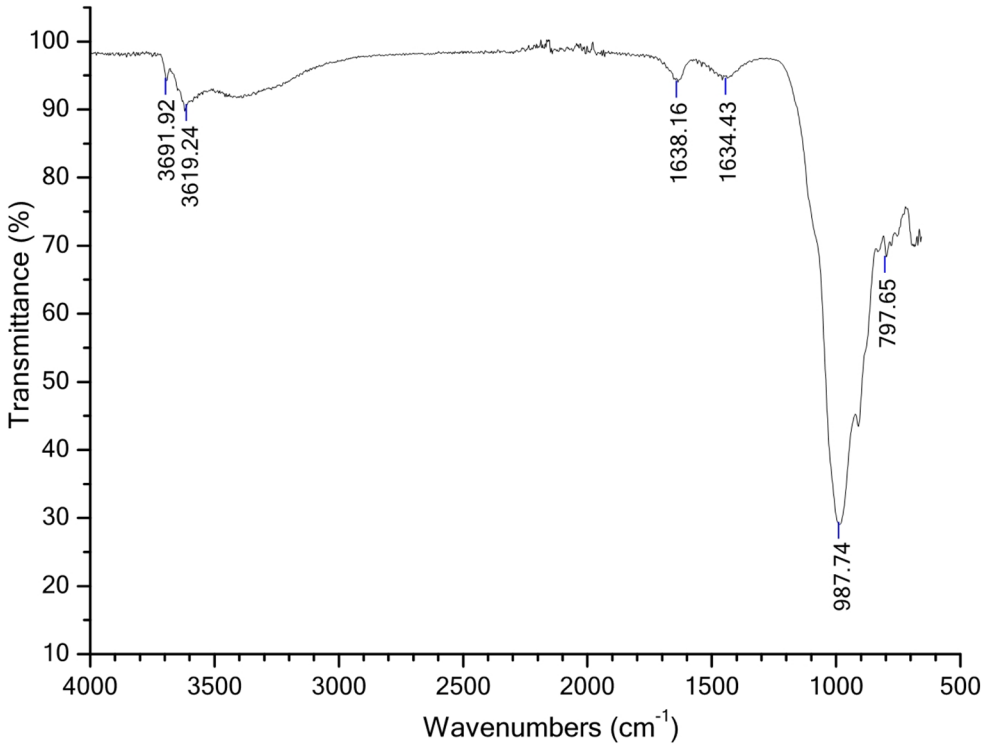

Fig. 4 FTIR spectra of green clay material

GCM. It shows that the total pore volume and the S_{BET} are 0.18 cm^3/g and 67 m^2/g, respectively.

6.2 Impact of Variation of Different Parameters on Fixed Bed Adsorption

The column adsorption experiments were conducted to investigate the effects of three parameters. Firstly, the initial concentration was varied at levels of 50, 75, and 100 mg/L. Secondly; the flow rate was adjusted to 3, 5, and 8 mL/min. Finally, the bed height was varied at different levels of 6, 9, and 12 cm. All experiments were carried out at 25 °C, and the initial pH of the solution was maintained at 5.

6.2.1 Effect of Initial Concentration

The impact of initial concentration (C_0) on the adsorption process was investigated by varying the desired concentration within the range of 50 to 100 mg/L. The flow rate (Q) and bed height (Z) were maintained at constant

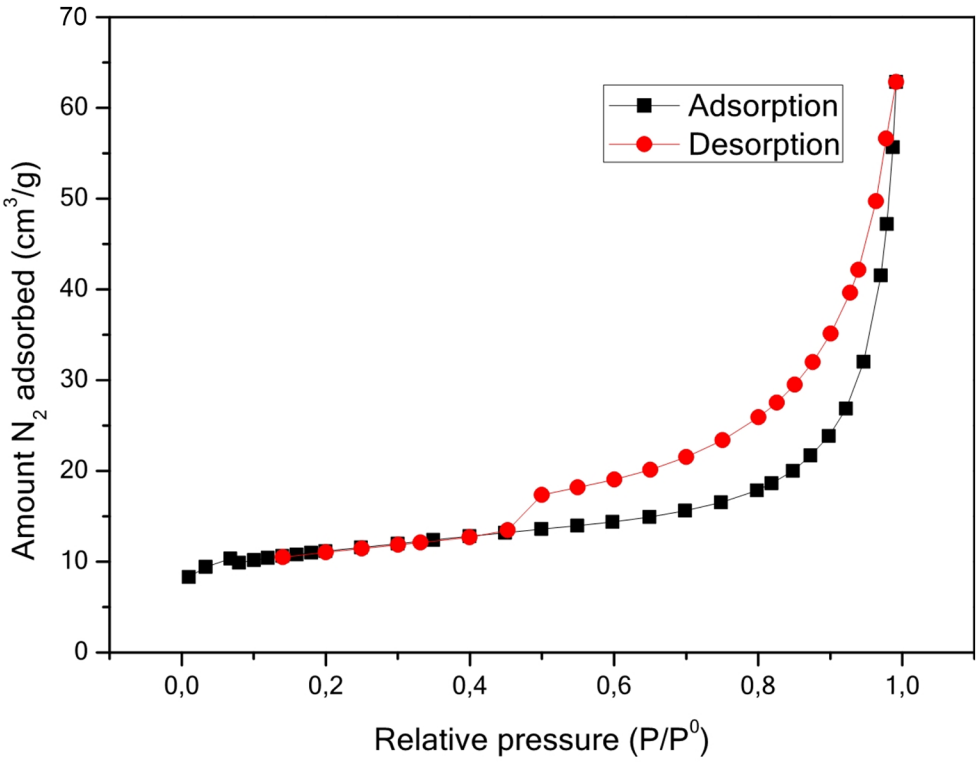

Fig. 5 N2 adsorption and desorption isotherms of green clay material

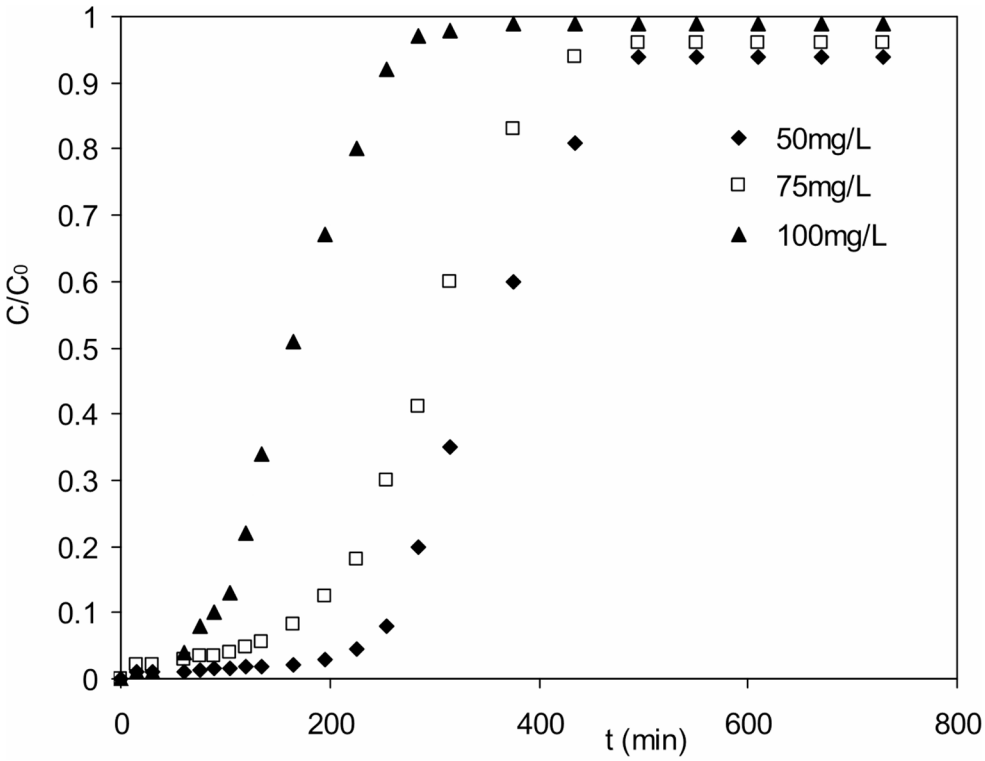

Fig. 6 Effect variation of Cr(VI) initial concentration (3 ml/min, 12 cm and 25 °C)

values of 3 mL/min and 12 cm, respectively. The results depicting breakthrough curves versus time are presented in Fig. 6. At a low concentration, the number of Cr (VI) ions exceeded the available sites on the GCM adsorbent, leading to both a delayed adsorption front and breakthrough time. With a higher concentration of Cr^{6+} ions in the solution (100 mg/L), the exhaustion time of the fixed bed column was achieved more rapidly compared to 50 mg/L (Fig. 6). This phenomenon can be attributed to the increased availability of metal ions at higher concentrations [64, 65]. These

ions readily occupy the active sites of the adsorbent within the packed bed, leading to a quicker exhaustion time [66, 67]. In contrast, at lower concentrations of Cr^{6+} ions, the process takes longer due to the limited availability of metal ions to occupy the active sites, resulting in a comparatively prolonged exhaustion time. Gizaw et al. [68] and Banchhor et al. [69] identified similar trends. In our study, a concentration of 50 mg/L proved to be the optimal level for recovering the maximum of the treated solution.

6.2.2 Effect of Flow Rate

The flow rate is a crucial factor in predicting the efficacy of the studied adsorbent. To investigate breakthrough curve behavior, the flow rate (Q) was varied between 3 and 8 mL/min, maintaining a constant concentration of 50 mg/L and a bed height of 12 cm. Figure 7 display breakthrough curves at different flow rates, revealing that breakthrough occurred more rapidly at higher flow rates. This acceleration may be attributed to the increased availability of reaction sites capable of capturing Cr^{6+} ions within or around the GCM adsorbent, compromising removal efficiency. At lower flow rates (3 mL/min), the GCM sample effectively removed Cr^{6+} ions, achieving a purification efficiency of 99% at approximately 180 min, consistent with Subair et al.'s findings in 2024 [25]. Conversely, at higher flow rates (8 mL/min), the pump injected more chromium solution into the bed, and active sites lacked sufficient time to trap ions. The heightened pump velocity could create channels in the packed bed [70, 71], facilitating the unhindered passage of Cr^{6+} ions and contributing to the lower breakthrough time at high flow rates. Consequently, the efficiency of the GCM bed in removing hexavalent chromium decreased with increasing flow rate.

6.2.3 Effect of Bed Height

To investigate the impact of bed height on the removal process, the GCM sample was packed at 6, 9, and 12 cm levels, maintaining a constant initial concentration (50 mg/L) and flow rate (3 mL/min). Figure 8 illustrates the relationship between C/C_0 and time at different fixed bed heights, highlighting that an increase in bed height corresponds to a higher percentage of purification and a delayed breakthrough time. According to Fig. 8, the optimal purification of hexavalent chromium was achieved at the 12 cm level of the column. This can be explained by the fact that the metal solution spends more residence time in the column at greater heights, allowing it more time to incorporate into the material's sites and facilitating removal from unsaturated sites. The obtained results emphatically confirm that the saturation time of the column is systematically dependent on the bed height [72, 73].

6.3 Interpretation of Breakthrough Curve Modeling

The experimental data were simulated using the Bohart-Adams model to determine the values of two parameters: maximum adsorption capacity (N_0) and mass transfer coefficient (k_{BA}), considering various inlet concentrations, bed heights, and hexavalent chromium flow rates. As depicted in Table 2, it was observed that the values of k_{BA} decreased

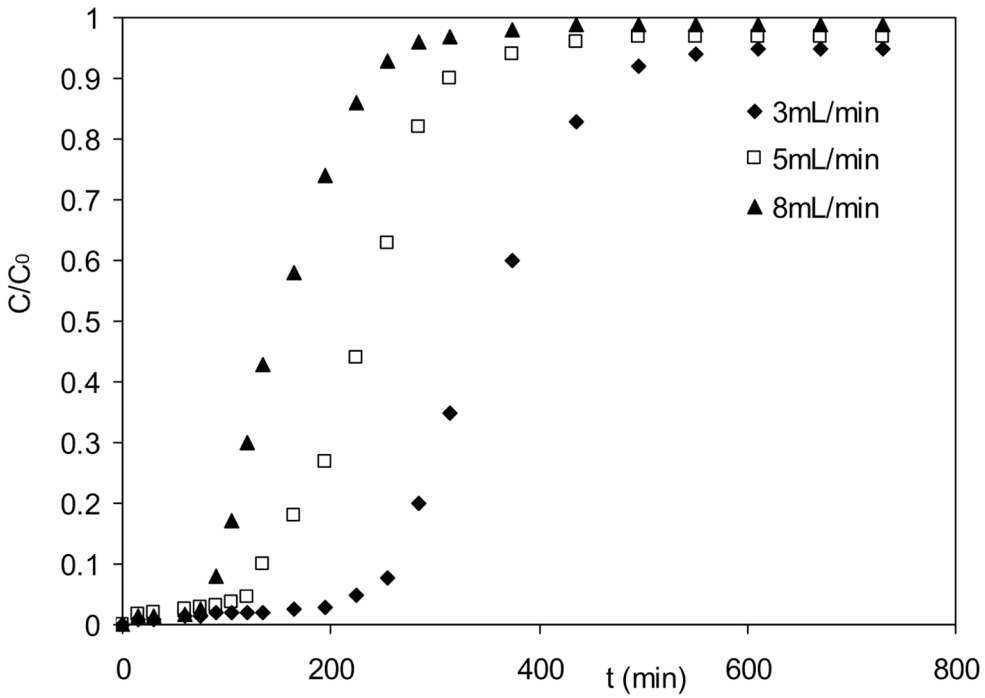

Fig. 7 Effect variation of flow rate of chromium solution (50 ml/L, 12 cm and 25 °C)

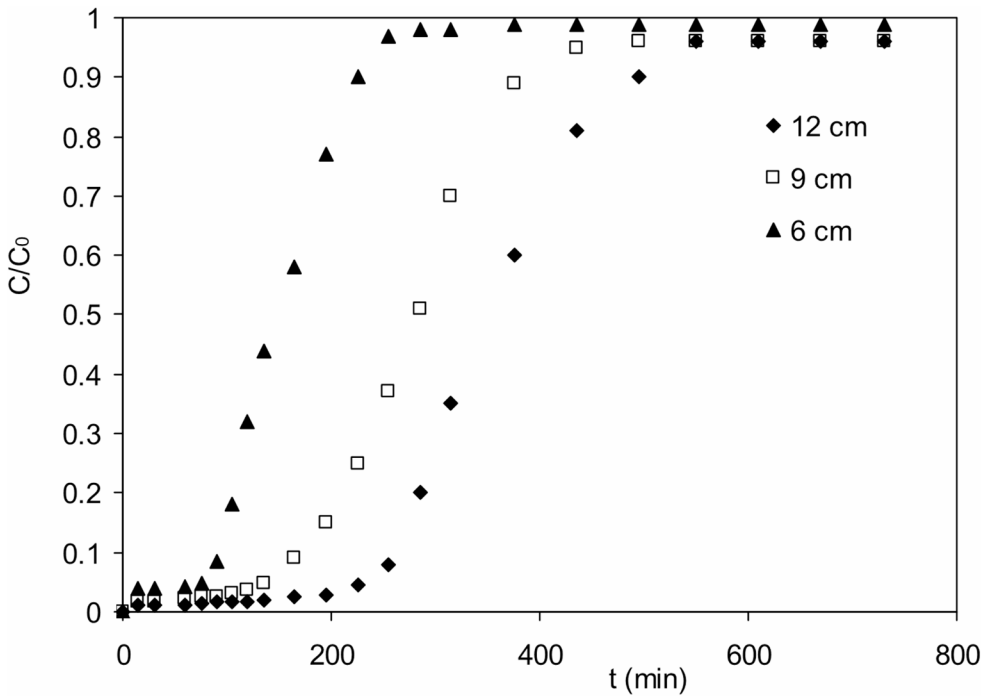

Fig. 8 Effect variation of bed height of clay and sand packed (50 ml/L, 3 ml/min and 25 °C)

Table 2 Constants of the Bohart-Adams, thomas, and Yoon-Nelson models were analyzed for the adsorption of hexavalent chromium by green clay material in a fixed-bed column

			Bohart-Adams			Yoon-Nelson			Thomas		
C_0 ($mg.L^{-1}$)	Q ($mL.min^{-1}$)	Z (cm)	k_{AB} ($L.mg^{-1}.min^{-1}$)	N_0 ($mg.L^{-1}$)	R^2	k_{YN} (min^{-1})	t_{50} (min)	R^2	kT ($mL.mg^{-1}.min^{-1}$)	q_0 ($mg.g^{-1}$)	R^2
50	3	12	$1.72\ 10^{-4}$	1293	0.672	0.019	356	0.998	0.375	3.178	0.998
75	3	12	$1.45\ 10^{-4}$	1356	0.750	0.018	298	0.995	0.345	2.389	0.997
100	3	12	$3.14\ 10^{-4}$	779	0.626	0.027	165	0.998	0.475	1.413	0.999
50	5	12	$3.14\ 10^{-4}$	1146	0.646	0.025	231	0.999	0.699	2.101	0.999
50	8	12	$6.68\ 10^{-4}$	1157	0.556	0.036	141	0.993	1.87	1.082	0.992
50	3	6	$5.20\ 10^{-4}$	925	0.855	0.032	151	0.996	0.599	2.424	0.996
50	3	9	$3.58\ 10^{-4}$	947	0.665	0.021	279	0.997	0.364	2.728	0.996

with increasing concentration and bed depth, indicating dominance of external mass transfer in the system's overall kinetics, while k_{BA} increased with higher hexavalent chromium flow rates. However, the values of N_0 did not exhibit a significant variation proportionate to the increase in inlet concentration of hexavalent chromium, flow rate, or bed depth. Additionally, the low regression values (R^2) ranging from 0.556 to 0.855 suggest that the Bohart-Adams model inadequately describes the mass transfer of hexavalent chromium in the GCM.

The adsorption capacity (q_0) and constant (k_{Th}) of the Thomas model were computed using the non-linear regression method. As shown in Table 2, the value of q_0 decreased from 2.728 to 1.413 $mg.g^{-1}$ as the inlet concentration of hexavalent chromium increased from 50 to 100 $mg.L^{-1}$. Additionally, the value of k_{Th} increased from 0.375 to 0.475 $mL.mg^{-1}.min^{-1}$. When the inlet flow rate increased from 3 to 8 $mL.min^{-1}$ (Table 2), k_{Th} values rose from 0.375 to 1.87 $mL.mg^{-1}.min^{-1}$, while q_0 decreased from 2.728 to 1.082 $mg.g^{-1}$. This trend aligns with findings by Da Costa et al. [53] regarding the adsorption of Cr(III) on alginate extraction residue (RES). However, with an increase in bed height from 6 to 12 cm, k_{Th} values decreased from 0.599 to 0.375 $mL.mg^{-1}.min^{-1}$. Correspondingly, q_0 values (Table 2) followed the same trend, ranging from 3.178 to 2.728 $mg.g^{-1}$, contrasting with findings for the adsorption of Cr(VI) onto SAAEF by Wang et al. [51]. The high compatibility of experimental data with the Thomas model (R^2 up to 0.999) suggests that internal and external diffusion are not limiting factors.

Table 2 presents the estimated values of k_{YN} (constant) and t50 (time required for a 50% breakthrough of hexavalent chromium) for the Yoon-Nelson model at various concentrations, bed heights, and hexavalent chromium flow rates. It has been observed that the values of k_{YN} increase with increasing concentration and flow rate, but decrease with

the bed height of the hexavalent adsorbate. The values of t50 increased from 151 to 356 min as the bed depth increased from 6 to 12 cm, but decreased from 356 to 165 min and from 356 to 141 min with the increase in concentration and flow rate, respectively. The decrease in t50 with increasing flow rate indicates that as the flow rate increases, the depletion rate of the GCM bed accelerates, which is undesirable for the adsorption process. These findings are consistent with those obtained by Da Costa et al. [53] for Cr(III) on RSE and Fakhfakh et al. [52] for o-xylene adsorption onto raw clay material. Moreover, the experimental data were well-described by the Yoon-Nelson model, with correlation coefficients ranging from 0.995 to 0.998.

Yoon-Nelson and Thomas models exhibit excellent fits with R^2 values ranging from 0.990 to 0.999. Consequently, for the clay material under study, including various concentrations of hexavalent chromium, bed heights, and flow rates, the complete penetration curve can be accurately defined by the Yoon-Nelson and Thomas models (Fig. 9).

6.4 Potential Application

Figure 10 clearly illustrates the evolution of the degree of purification under optimal conditions, providing insights into the progression of clay capacity as a chromium adsorption agent. It highlights crucial factors, including breakthrough time, clay saturation, and the influence of parameter variations on the adsorption process.

At the onset of the experiment, the breakthrough time is prolonged and significant, signifying that the clay requires time to initiate the retention of chromium ions present in the solution. This extension may be attributed to the time needed for the clay's active sites to become available for adsorption.

The increase in chromium's initial concentration, flow rate, and the decrease in column height collectively contribute to a reduction in breakthrough time. This suggests that these parameters facilitate a more rapid adsorption of chromium onto the GCM.

In the initial hours, particularly within the first three hours, the purification percentage reaches 100% (Fig. 10a). This accomplishment indicates that the clay efficiently adsorbs chromium ions from the solution, delivering a high level of purification in a relatively short timeframe.

After twelve hours, the purification percentage drops to zero, implying that the chromium concentration at the column outlet equals that at the inlet ($C = C_0$) (Fig. 10b). This indicates that the clay is saturated with chromium ions, and the active sites can no longer adsorb free chromium. At this stage, the efficiency of the clay as a chromium adsorption agent significantly decreases, rendering it incapable of effectively purifying the solution.

The obtained results encourage the utilization of treated water in various industrial activities, especially in car cleaning, bricks production and bioelectricity production through green plants, hydrogen production, even also secondary domestic use, etc.

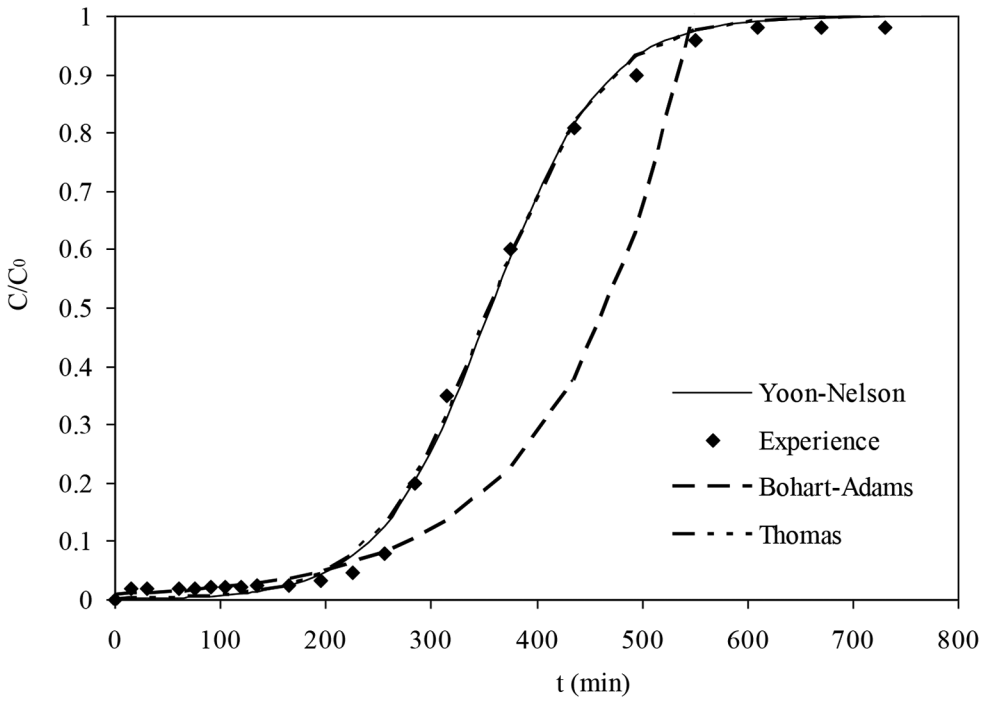

Fig. 9 Modeling breakthrough curve of hexavalent chromium adsorption in fixed bed (under the following optimal experimental conditions: initial concentration 50 mg/L, flow rate 3mL/min, and bed height 12 cm)

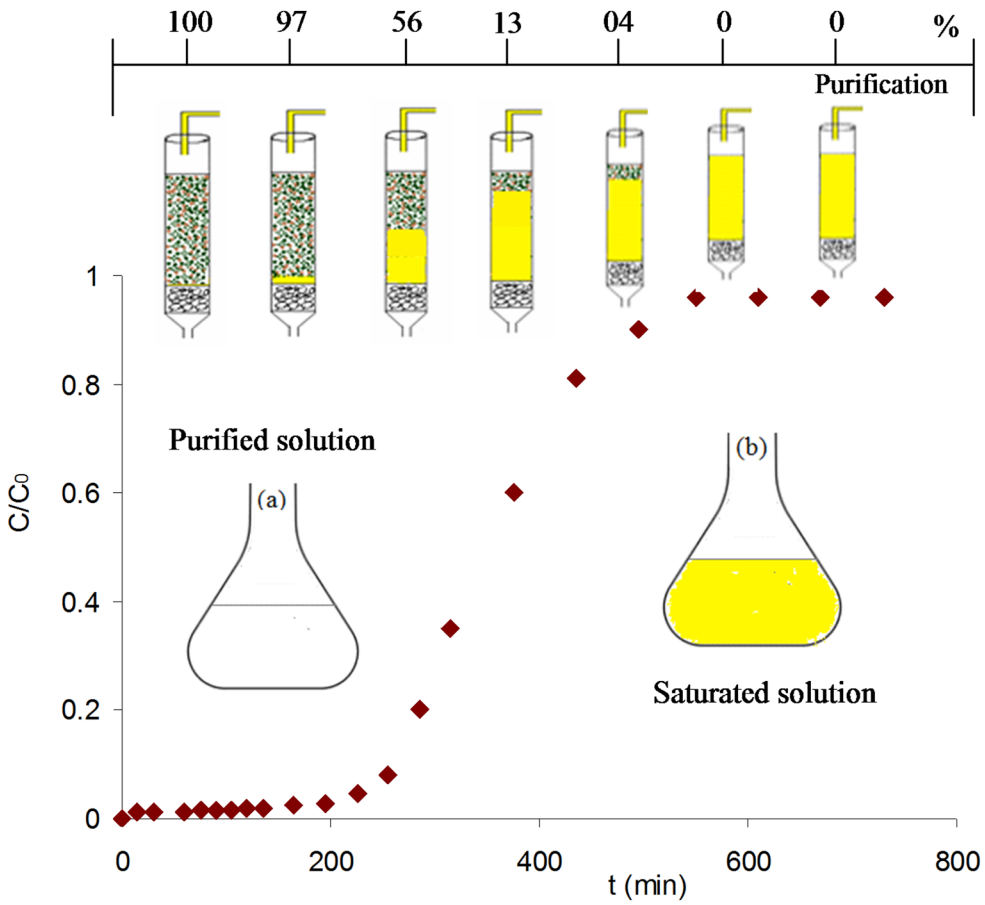

Fig. 10 Efficiency of GCM in Cr(VI) purification and its potential environmental and industrial applications (50 ml/L, 3 ml/min, 12 cm and 25 °C)

Table 3 Comparative studies on Cr(VI) adsorption capacities of different adsorbents

Different adsorbents	Adsorption capacity ($mg.g^{-1}$)	Reference
Activated zeolite	3.59	[74]
Cashew nutshell	3.12	[75]
Neutralized activated red mud	3.81	[23]
Silver nanoparticle-maize leaf composite	3.14	[76]
Acid modified bentonite clay	2.46	[77]
Green clay material	3.17	Present study

6.5 Comparison Cr(VI) Adsorption Capacity Behavior with Other Studies

Several studies have experimented with various natural and modified adsorbents for continuous fixed-bed chromium ion adsorption. We compared the findings of this present work with similar studies conducted under the same conditions in a dynamic system. This comparison showed that the green clay material performed better and exhibited a similar adsorption capacity to other adsorbents, as shown in Table 3. It can be concluded that the low cost and effectiveness of the studied material make it suitable for widespread use in environmental or industrial applications.

7 Regeneration of GCM

The GCM was regenerated to make the process more practical and cost-effective, significantly improving the overall economy of the procedure. The stability of the GCM was evaluated in four consecutive tests using traditional regeneration with an N_2 flow. Between experiments, the GCM was filtered, thoroughly rinsed with distilled water, and dried for 12 h at 60 °C. The clay was placed inside a 75 cm long, 10 cm I.D. cylinder, which was externally heated using a tube furnace. Before activating the electric heater, the cylinder was sealed at both ends and purged with N_2 gas for 10 min to ensure the complete removal of air. Regeneration tests lasting over two hours were conducted to assess temperatures up to 200 °C.

As the number of recycling increased, the removal efficiency of the GCM slightly decreased, as shown in Fig. 11. By the fourth cycle, 80% of the material had been removed. These results indicate that green clay material can be reused over multiple cycles.

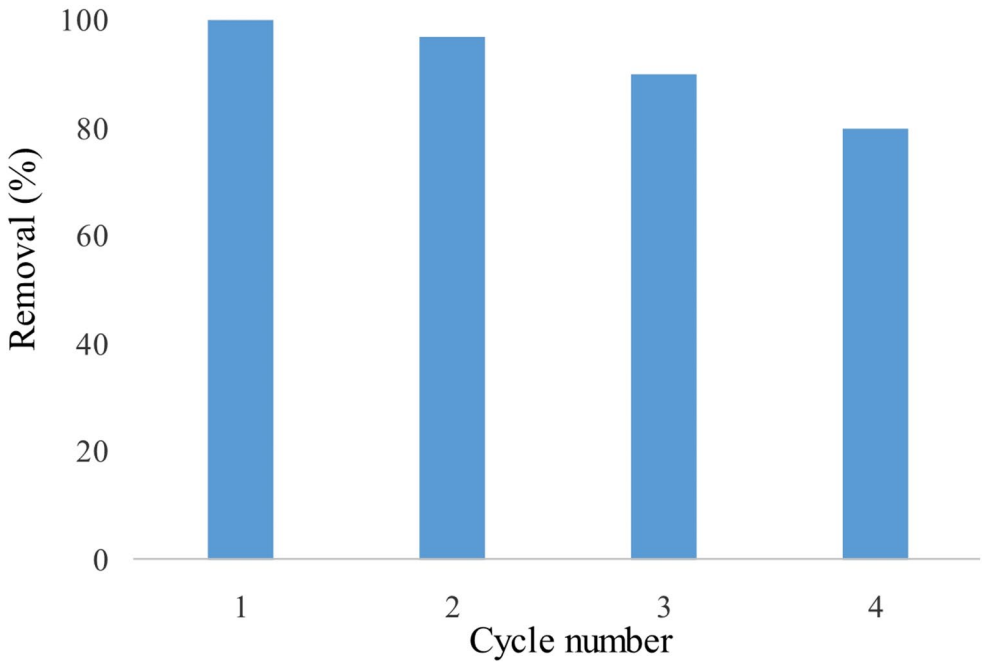

Fig. 11 Reusability of GCM for multiple cycles

8 Conclusions

A clean technology for hexavalent chromium purification utilizing natural illitic clay in laboratory packed column conditions was developed and assessed. The efficiency of this environmentally friendly material in purifying contaminated solutions was systematically evaluated. The adsorbent demonstrated effective performance in continuously operating packed columns at both laboratory and pilot scales, adapting well to varying operating conditions, including concentration, effluent flow, and bed height.

In the laboratory, the adsorbent displayed an average adsorption capacity of 3.178 mg/g. A purification percentage of 100% was attained in an aqueous solution with an initial concentration of 50 mg/L, operating at a flow rate of 3 mL/min and a packed bed height of 12 cm. The impact of initial concentration, flow rate and packed bed height became apparent in the column breakthrough and saturation time, directly influencing the purification percentage. Specifically, an increase in bed height extended both the breakthrough and saturation times.

This study utilized three models: Bohart-Adams, Thomas and Yoon-Nelson to describe the breakthrough curves. Through a comparison between experimental and calculated data, the Yoon-Nelson and Thomas models proved to be suitable for scaling up the chromium adsorption process in a packed bed column. The findings from our study suggest that the proposed natural and cost-effective adsorbent material holds potential for the industrial-scale purification of heavy metal-rich wastewater.

Acknowledgements The authors sincerely thank Mlle Amina Zineddine, a technician at the National School of Engineering of Sfax, for her assistance in facilitating the DRX and FTIR analyses. Additionally, the authors express their gratitude to the anonymous reviewers for their insightful suggestions, which have significantly contributed to enhancing the manuscript.

Author Contributions Conceptualization, funding acquisition, and writing: Mabrouk Eloussaief. Software, formal analysis and investigation: Nesrine Dammak. Data acquisition and sample collecting: Sana Ghrab, Olfa Ouled Ltaief and Wiem Hamza. Manuscript review and supervision: Stephanie Lambert, Hicham Zaitan and Mourad Benzina.

Data Availability We confirm that all data supporting the findings of this work are available within this publication and can be accessed by all readers.

Declarations

Conflict of Interest The authors declare the absence of any known conflicts of interest related to this publication, and there has been no substantial financial support for this work that could potentially influence its outcome.

References

1. Silva LF, Vallejuelo SFO, Martinez-Arkarazo I, Castro K, Oliveira ML, Sampaio CH, Madariaga JM (2013) Study of environmental pollution and mineralogical characterization of sediment rivers from Brazilian coal mining acid drainage. Sci Total Environ 447:169–178
2. Dutta M, Islam N, Rabha S, Narzary B, Bordoloi M, Saikia D, Saikia BK (2019) Acid mine drainage in an Indian high-sulfur coal mining area: Cytotoxicity assay and remediation study J. Hazard Mater 389:121851

3. Svetlana B, Plamen T (2024) Migration of heavy metals from mine waste rock dump end environmental impact on groundwaters and sediments. J Chem Technol Metall 59:145–156
4. Jiang B, Liu Y, Zheng J, Tan M, Wang Z, Wu M (2015) Synergetic transformations of multiple pollutants driven by Cr (VI)-sulfite reactions. Environ Sci Technol 49:12363–12371
5. Ball JW, Izbicki JA (2004) Occurrence of hexavalent chromium in ground water in the western Mojave Desert, California. Appl Geochem 19:1123–1135
6. Vaiopoulou E, Gikas P (2020) Regulations for chromium emissions to the aquatic environment in Europe and elsewhere. Chemosphere 254:126876. https://doi.org/10.1016/j.chemosphere.2020.126876
7. Kundu D, Dutta D, Joseph A, Jana A, Samanta P, Bhakta JN, Alreshidi MA (2024) Safeguarding drinking water: A brief insight on characteristics, treatments and risk assessment of contamination. Environ Monit Assess 196:180. https://doi.org/10.1007/s10661-024-12311-z
8. Sharma P, Singh SP, Parakh SK, Tong YW (2022) Health hazards of hexavalent chromium (Cr (VI)) and its microbial reduction. Bioengineered 13:4923–4938. https://doi.org/10.1080/21655979.2022.2037273
9. Gning A, Gaye C, Kama A, Diaw P, Thiare D, Fall M (2024) Hexavalent Chromium Cr (VI) Removal from Water by Mango Kernel Powder. J Chem Eng Mater Sci 12:84–103. https://doi.org/10.4236/msce.2024.121007
10. Karthik Ch, Elangovan N, Kumar TS, Govindharaju S, Barathi S, Ovesc M, Arulselvi PI (2017) Characterization of multifarious plant growth promoting traits of rhizobacterial strain AR6 under Chromium (VI) stress. Microbio Res 204:65–71. https://doi.org/10.1016/j.micres.2017.07.008
11. Prasad S, Yadav KK, Kumar S, Gupta N, Marina. Cabral Pinto MS, Rezania S, Radwan N, Alam J (2021) Chromium contamination and effect on environmental health and its remediation: A sustainable approaches. J Environ Manage 285:112174. https://doi.org/10.1016/j.jenvman.2021.112174
12. Alur A, Phillips J, Xu D (2024) Effects of hexavalent chromium on mitochondria and their implications in carcinogenesis. J Environ Sci Health C: Toxicol. https://doi.org/10.1080/26896583.2024.2301899
13. Chen D, Cheng Y, Zhou N, Chen P, Wang Y, Li K, Huo S, Cheng P, Peng P, Zhang R, Wang L (2020) Photocatalytic degradation of organic pollutants using TiO2-based photocatalysts: a review. J Clean Prod 268:121725. https://doi.org/10.1016/j.jclepro.2020.121725
14. Qasem NAA, Mohammed RH, Lawal DU (2021) Removal of heavy metal ions from wastewater: a comprehensive and critical review. npj Clean Water 4:36. https://doi.org/10.1038/s41545-021-00127-0
15. Saha B, Amine A, Verpoort F (2022) Hexavalent Chromium: Sources, Toxicity, and Remediation. Chem Afr 5:1779–1780. https://doi.org/10.1007/s42250-022-00443-z
16. Grzegorzek M, Wartalska K, Kaźmierczak B (2023) Review of water treatment methods with a focus on energy consumption. Int Commun Heat Mass Transf 143:106674. https://doi.org/10.1016/j.icheatmasstransfer.2023.106674
17. Yang M (2024) Performance and mechanism of Cr(VI) removal by sludge-based biochar loaded with zero-valent iron. Desalin Water Treat 317:100035. https://doi.org/10.1016/j.dwt.2024.100035
18. Mohammed N, Grishkewich N, Waeijen HA, Berry RM, Tam KC (2016) Continuous flow adsorption of methylene blue by cellulose nanocrystal-alginate hydrogel beads in fixed bed columns. Carbohyd Polym 136: 1194–202. https://doi.org/10.1016/jcarbpol. 2015. 09. 099
19. Sallam A, Al-Zahrani M, Al-Wabel M, Al-Farraj A, Usman A (2017) Removal of Total chromium and Toxic Ions from Aqueous Solutions and Tannery Wastewater Using Polymer-Clay Composites. Sustainability 9:11–1993. https://doi.org/10.3390/su9111993
20. Yousefi M, Nabizadeh R, Alimohammadi M, Mohammadi AA, Mahvi AH (2019) Removal of phosphate from aqueous solutions using granular ferric hydroxide process optimization by response surface methodology. Desalin Water Treat 158:290–300
21. Sasidharan V, Georgin J, Dison SPF, Meili L, Singh P, Jawad AH, Selvasembian R (2022) Hexavalent chromium adsorption onto environmentally friendly mesquite gum–based polyurethane foam. Biomass Convers Biorefin. https://doi.org/10.1007/s13399-022-03528-4
22. Patel H (2019) Fixed–bed column adsorption study: a comprehensive review. Appl Water Sci 9–45. https://doi.org/10.1007/s13201-019-0927-7
23. Giri AK, Mishra PC (2022) Application of artificial neural network for prediction of fluoride removal efficiency using neutralized activated red mud from aqueous medium in a continuous fixed bed column. Environ Sci Pollut Res 30:23997–24012. https://doi.org/10.1007/s11356-022-23593-6
24. Gholamifard H, Rasul MG, Rahideh H, Azari A, Abbasi M, Karami R (2023) Experimental and numerical analysis of oily wastewater treatment using low-cost mineral adsorbent in a single and multi-fixed bed column. Chem Eng J Adv 16:100551. https://doi.org/10.1016/j.ceja.2023.100551
25. Subair A, Lakshmi PK, Chellappan S, Chinghakham C (2024) Removal of polystyrene microplastics using biochar–based continuous fow fxed–bed column. Environ Sci Pollut Res. https://doi.org/10.1007/s11356-024-32088-5
26. Wang G, Hua Y, Su X, Komarneni S, Ma S, Wang Y (2016) Cr(VI) adsorption by montmorillonite nanocomposites. Appl Clay Sci 124:111–118. https://doi.org/10.1016/j.clay.2016.02.008
27. Ashour EA, Tony MA (2020) Eco–friendly removal of hexavalent chromium from aqueous solution using natural clay mineral: activation and modification effects. SN Appl. Sci 2: 2042. https://doi.org/10.1007/s42452-020-03873-x
28. Aziri S, Meziane S, Bozetine H, Berkane N (2024) Taguchi method for optimization of Cr(VI) removal, isotherm, kinetic and thermodynamic studies. Nucleosides Nucleotides Nucleic Acids. https://doi.org/10.1080/15257770.2024.2308517
29. Kainth S, Sharma P, Pandey OP (2024) Green sorbents from agricultural wastes: A review of sustainable adsorption materials. Appl Surf Sci Adv 19:100562. https://doi.org/10.1016/j.apsadv.2023.100562
30. Guerra DL, Oliveira CPH, da Costa PCC, Rúbia RV, Airoldi C (2010) Adsorption of chromium (VI) ions on Brazilian smectite: Effect of contact time, pH, concentration, and calorimetric investigation. CATENA 82:35–44
31. Dasgupta S, Das M, Klunk MA, Xavier SJS, Caetano NR, Wander PR (2021) Copper and chromium removal from synthetic textile wastewater using clay minerals and zeolite through the effect of pH. J Iran Chem Soc 18:3377–3386. https://doi.org/10.1007/s13738-021-02273-1
32. El Nemr A, Ismail M, El Ashry HES, Abdel Hamid H (2020) Novel simple modifcation of chitosan as adsorptive agent for removal of Cr6 + from aqueous solution. Egypt J Chem 63:21–22
33. Mancilla HB, Cerrón MR, Aroni PG, Paucar JE-P, Tovar CT, Jindal MK, Gowrisankar G (2022) Effective removal of Cr (VI) ions using low–cost biomass leaves (Sambucus nigra L.) in aqueous solution. Environ Sci Pollut Res 30:106982–106995. https://doi.org/10.1007/s11356-022-24064-8
34. Yüksel Ş, Orhan R (2019) The Removal of Cr(VI) from Aqueous Solution by Activated Carbon Prepared from Apricot, Peach Stone and Almond Shell Mixture in a Fixed-Bed Column. Arab J Sci Eng 44:5345–5357. https://doi.org/10.1007/s13369-018-3618-z
35. Sharififard H, Boostani F, Fateminia FS, Kalantari N (2012) Activated carbon from local oak shells: synthesis, characterisation,

and application for Cr (VI) adsorption in the fixed bed column: Experimental and modelling. J. Environ. Anal. Chem 104: 178–197. https://doi.org/10.1080/03067319.2021.2018425
36. Pereira L, Castillo V, Calero M, Blázquez G, Solís RR, Martín-Lara MA (2024) Conversion of char from pyrolysis of plastic wastes into alternative activated carbons for heavy metal removal. Environ Res 250:118558. https://doi.org/10.1016/j.envres.2024.118558
37. Esmaeili A, Mobini M, Eslami H (2019) Removal of heavy metals from acid mine drainage by native natural clay minerals, batch and continuous studies. Appl Water Sci 9:97. https://doi.org/10.1007/s13201-019-0977-x
38. Khan S, Ajmal S, Hussain T, Rahman MU (2023) Clay-based materials for enhanced water treatment: adsorption mechanisms, challenges, and future directions. J Umm Al-Qura Univ Appl Sci. https://doi.org/10.1007/s43994-023-00083-0
39. Zhang T, Wang W, Zhao Y, Bai H, Wen T, Kang S, Song G, Song S, Komarneni S (2020) Removal of heavy metals and dyes by clay-based adsorbents: from natural clays to 1D and 2D nanocomposites. Chem Eng J 420:127574. https://doi.org/10.1016/j.cej.2020.127574
40. Andrunik M, Bajda T (2019) Modification of Bentonite with Cationic and Nonionic Surfactants: Structural and Textural Features. Materials 12:3772
41. Razzak SA, Faruque MO, Alsheikh Z, Alsheikhmohamad L, Alkuroud D, Alfayez A, Zakir Hossain SM-Z, Hossain MM (2022) A comprehensive review on conventional and biological-driven heavy metals removal from industrial wastewater. Environ Adv 7:100168. https://doi.org/10.1016/j.envadv.2022.100168
42. Topare NS, Wadgaonkar VS (2023) A review on application of low-cost adsorbents for heavy metals removal from wastewater. Materials Today: Proceedings 1:8–18. https://doi.org/10.1016/j.matpr.2022.08.450
43. Bouaziz S (1995) Étude de la tectonique cassante dans la plateforme et l'Atlas saharien (Tunisie méridionale): évolution des paléochamps de contraintes et implications géodynamiques, thèse d'État, faculté des sciences de Tunis, université Tunis-2, Tunis. 1995, 485 p
44. Jamoussi F (2001) Les argiles de Tunisie: étude minéralogique, géochimique, géotechnique et utilisations industrielles, thèse d'État, faculté des sciences de Tunis, université Tunis-El- Manar, 437 p
45. Sdiri A, Khairy M, Bouaziz S, El-Safty S (2016) A natural clayey adsorbent for selective removal of lead from aqueous solutions. Appl Clay Sci 126:89–97
46. Abdeljaoued S, Zargouni F (1981) Mise en évidence d'une tectonique intra crétacée dans le secteur de Jebel Zemlet El Beida (chaîne nord des Chotts). Acte du 1er Congr. Nat Sc Terre t 1:285
47. Ouled Ltaief O, Fourmentin S, Sifert S, Benzina M (2024) Preparation of powerful exchanged Faujasite zeolite materials used as efective heterogeneous catalyst for photo–Fenton oxidation of methyl orange (MO). React Kinet Mech Catal 137:547–570. https://doi.org/10.1007/s11144-023-02563-0
48. Eloussaief M, Jarraya I, Benzina M (2009) Adsorption of copper ions on two clays from Tunisia: pH and temperature effects. Appl Clay Sci 46:409–413
49. Onchoke KK, Sasu SA (2016) Determination of Hexavalent Chromium (Cr(VI)) Concentrations via Ion Chromatography and UV-Vis Spectrophotometry in Samples Collected from Nacogdoches Wastewater Treatment Plant, East Texas (USA). Adv Environ Res 3468635:10. https://doi.org/10.1155/2016/3468635
50. Aksu Z, Gonen F (2004) Biosorption of phenol by immobilized activated sludge in a continuous packed bed: prediction of breakthrough curves. Process Biochem 39:599–613
51. Wang W, Li M, Zeng Q (2015) Adsorption of chromium (VI) by strong alkaline anion exchange fiber in a fixed-bed column: Experiments and models fitting and evaluating. Sep Purif Technol 149:16–23
52. Fakhfakh N, Dammak N, Benzina M (2017) Breakthrough modeling and experimental design for o-xylene dynamic adsorption onto clay material. Environ Sci Pollut Res https://doi.org/10.1007/s11356-017-9386-6
53. Da Silva costaTB, Dias Costa TL, Da Silva CS, Adeodato Vieira MGC MG (2022) Chromium adsorption using Sargassum filipendula algae waste from alginate extraction: Batch and fixed-bed column studies. Chem Eng J Adv 11:100341
54. [54] Bohart and, Adams G (1920) Some aspects of the behavior of charcoal with respect to chlorine. J Am Chem Soc 42:523–544
55. Sdiri A, Higashi T, Hatta T, Jamoussi F, Tase N (2010) Mineralogical and spectroscopic characterization, and potential environmental use of limestone from the Abiod formation, Tunisia. Environ Earth Sci 61:1275–1287. https://doi.org/10.1007/s12665-010-0450-5
56. Ghrab S, Mefteh S, Medhioub M, Benzina M (2018) Adsorption of nickel (II) and chromium(III) from aqueous phases on raw smectite: kinetic and thermodynamic studies. Arab J Geosci 11:440. https://doi.org/10.1007/s12517-018-3749-2
57. Eloussaief M, Chakroun S, Kallel N, Benzina M (2020) Efficiency of clay materials collected from Ain Jaloula (Central Tunisia) in sunflower oil decolorization. EuroMediterr J Environ Integr 5:33. https://doi.org/10.1007/s41207-020-00171-1
58. Oumar KO, Gilbert François NN, Bertrand MM, Nathanael T, Constantin BE, Simon MJ, Jacques E (2022) Mineralogical, Geochemical Characterization and Physicochemical Properties of Kaolinitic Clays of the Eastern Part of the Douala Sub-Basin, Cameroon, Central Africa. Appl Sci 12:9143. https://doi.org/10.3390/app12189143
59. Di Pietro SA, Emerson HP, Katsenovich YP, Johnson TJ, Francis RM, Mason HE, Marple MA, Sawvel AM, Szecsody JE (2022) Solid phase characterization and transformation of illite mineral with gas-phase ammonia treatment. J Hazard Mater 424:127657. https://doi.org/10.1016/j.jhazmat.2021.127657
60. Hussain ST, Khaleefa Ali SA (2020) Removal of Heavy Metal by Ion Exchange Using Bentonite Clay. J Ecol Eng 22:104–111
61. Omer OS, Hussein B-HM, Ouf AM, Hussein MA, Mgaidi A (2018) An organified mixture of illite-kaolinite for the removal of Congo red from wastewater. J Taibah Univ Sci 12:858–866. https://doi.org/10.1080/16583655.2018.1540179
62. Dinh VP, Nguyen PT, Tran MC, Luu AT, Hung NQ, Luu TT, Kiet HAT, Mai XT, Luong TB, Nguyen TL, Nguyen DK, Pham DK, Hoang QA, Le TV, Nguyen TC (2022) HTDMA-Modified Bentonite Clay for Effective Removal of Pb(II) from aqueous solution. Chemosphere. https://doi.org/10.1016/j.chemosphere.2021.131766
63. Kgabi DP, Ambushe AA (2023) Characterization of South African Bentonite and Kaolin Clays. Sustainability 15:17–12679. https://doi.org/10.3390/su151712679
64. Badessa TS, Wakuma E, Yimer AM (2020) Bio-sorption for effective removal of chromium (VI) from wastewater using Moringa stenopetala seed powder (MSSP) and banana peel powder (BPP). BMC Chem 14:1–12. https://doi.org/10.1186/s13065-020-00724-z
65. Shankar P, Thandapani G, Kumar V, Narayanan SP (2022) Evaluation of batch and packed bed adsorption column for chromium (VI) ion removal from aqueous solution using chitosan-silica-g-AM/orange peel hydrogel composite, Biomass Convers. Biorefinery 14:2745–2760. https://doi.org/10.1007/s13399-022-02450-z
66. Banerjee M, Bar N, Basu RK, Das SK (2017) Comparative study of adsorptive removal of Cr(VI) ion from aqueous solution in fixed bed column by peanut shell and almond shell using empirical models and ANN. Environ Sci Pollut Res Int 24:10604–10620. https://doi.org/10.1007/s11356-017-8582-8

67. Kumar S, Patra C, Narayanasamy S, Rajaraman PV (2020) Performance of acid-activated water caltrop (Trapa natans) shell in fixed bed column for hexavalent chromium removal from simulated wastewater. Environ Sci Pollut Res 27:28042–28052. https://doi.org/10.1007/s11356-020-09155-8
68. Gizaw A, Zewge F, Chebude Y, Mekonnen A, Tesfaye M (2022) Simultaneous Nitrate and Phosphate Abatement Using Calcium Silicate Hydrate Adsorbent: Fixed Bed Column Adsorption Study. Surf Interfaces. https://doi.org/10.1016/j.surfin.2022.101961
69. Banchhor A, Pandey M, Pandey PK (2023) Adsorption of hexavalent chromium by Simarouba glauca in a fixed-bed column: a full-factorial design and mathematical modelling. Int J Environ Anal Chem. https://doi.org/10.1080/03067319.2023.2251418
70. Deokar SK, Mandavgane SA, Kulkarni BD (2016) Agro-industrial waste: a low cost adsorbent for effective removal of 4-chloro-2-methylphenoxyacetic acid herbicide in batch and packed bed modes. Environ Sci Pollut Res 23:16164–16175. https://doi.org/10.1007/s11356-016-6769-z
71. Patel H (2022) Comparison of batch and fixed bed column adsorption: a critical Review. Int J Environ Sci Technol 19:10409–10426. https://doi.org/10.1007/s13762-021-03492-y
72. Guerra DJL, Mello I, Freitas LR, Resende R, Silva RAR (2014) Equilibrium, thermodynamic, and kinetic of Cr(VI) adsorption using a modified and unmodified bentonite clay. Int J Min Sci Technol 24:525–535. https://doi.org/10.1016/j.ijmst.2014.05.017
73. Velarde L, Nabavi MS, Escalera E, Antti M-L, Akhtar F (2023) Adsorption of heavy metals on natural zeolites: A review. Chemosphere J. https://doi.org/10.1016/j.chemosphere.2023.138508
74. Yahya MD, Aliyu AS, Obayomi KS, Olugbenga AG, Abdullahi UB (2020) Column adsorption study for the removal of chromium and manganese ions from electroplating wastewater using cashew nutshell adsorbent. Cogent Eng 7:11748470. https://doi.org/10.1080/23311916.2020.1748470
75. Sanzana S, Abreua NJ, Levío-Raiman M, N´ajera JP, Osorio A, Maza S, Daniele L, Castro-Rojas J, Soto V, Gonz´alez C, Antileo C (2024) Enhancing manganese sorption: Batch and fixed-bed column studies on activated zeolite. Environ Technol Innov 33:103495. https://doi.org/10.1016/j.eti.2023.103495
76. Omitola OB, Abonyi MN, Akpomie KG, Dawodu FA (2022) Adams–Bohart, Yoon–Nelson, and Thomas modeling of the fix–bed continuous column adsorption of amoxicillin onto silver nanoparticle–maize leaf composite. Appli Water Sci 12:94. https://doi.org/10.1007/s13201-022-01624-4
77. Kalsido AW, Meshesha BT, Behailu BM, Alemayehu E (2021) Optimization of Fluoride Adsorption on Acid Modified Bentonite Clay Using Fixed-Bed Column by Response Surface Method. Molecules 26(23):7112. https://doi.org/10.3390/molecules26237112PMID: 34885692; PMCID: PMC8658911